Chaos, Solitons and Fractals 119 (2019) 8–18

Contents lists available at ScienceDirect

Chaos, Solitons and Fractals

Nonlinear Science, and Nonequilibrium and Complex Phenomena

journal homepage: www.elsevier.com/locate/chaos

Frontiers

Ordinal synchronization: Using ordinal patterns to capture interdependencies between time series☆

I. Echegoyen[a,b], V. Vera-Ávila[c], R. Sevilla-Escoboza[c], J.H. Martínez[d,b], J.M. Buldú[a,b,*]

[a] Laboratory of Biological Networks, Centre for Biomedical Technology., Universidad Politécnica de Madrid, Spain
[b] Complex Systems Group & G.I.S.C., Universidad Rey Juan Carlos, Móstoles, Spain
[c] Centro Universitario de Los Lagos, Universidad de Guadalajara, Lagos de Moreno, Mexico
[d] INSERM-UM1127, Sorbonne Université, ICM-Hôpital Pitié Salpêtrière, Paris, France

ARTICLE INFO

Article history:
Received 27 August 2018
Revised 5 November 2018
Accepted 10 December 2018
Available online 19 December 2018

Keywords:
Synchronization
Ordinal patterns
In-phase synchronization
Anti-phase synchronization
Nonlinear electronic circuits
Brain imaging data sets.

ABSTRACT

We introduce Ordinal Synchronization (*OS*) as a new measure to quantify synchronization between dynamical systems. *OS* is calculated from the extraction of the ordinal patterns related to two time series, their transformation into *D*-dimensional ordinal vectors and the adequate quantification of their alignment. *OS* provides a fast and robust-to noise tool to assess synchronization without any implicit assumption about the distribution of data sets nor their dynamical properties, capturing in-phase and anti-phase synchronization. Furthermore, varying the length of the ordinal vectors required to compute *OS* it is possible to detect synchronization at different time scales. We test the performance of *OS* with data sets coming from unidirectionally coupled electronic Lorenz oscillators and brain imaging datasets obtained from magnetoencephalographic recordings, comparing the performance of *OS* with other classical metrics that quantify synchronization between dynamical systems.

1. Introduction

Since the seminal work of Huygens about the coordinated motion of two pendulum clocks (refereed to as “an odd kind of sympathy”) [1], the study of synchronization in real systems has been one of the major research lines in nonlinear dynamics. From fireflies to neurons, synchronization has been reported in a diversity of social (e.g., human movement or clapping) [2,3], biological (e.g., brain regions or cardiac tissue) [4,5] and technological systems (e.g., wireless communications or power grids) [6,7], being in many cases a fundamental process for the functioning of the underlying system. However, despite being an ubiquitous phenomenon, the detection and quantification of synchronization can be a difficult task. The main reasons are the diversity of kinds of synchronization [8], the complexity of interaction between dynamical systems [9], the existence of unavoidable external perturbations [10] or the inability of observing all variables of a real system [11], just to name a few.

As a consequence, there is not a unique way of quantifying the amount of synchronization in real time series and a series of metrics have been proposed with this purpose. As a rough approximation, these metrics can be classified into three main groups: (i) linear, (ii) nonlinear and (iii) spectral metrics. While linear metrics, such as the Pearson correlation coefficient, are the most straightforward to be calculated and less time consuming, they suppose the existence of a linear correlation between time series, an assumption that is not fulfilled in the majority of real cases. On the other hand, nonlinear metrics asume a certain nonlinear coupling function f_n between a variable X and a variable Y, such as $X = f_n(Y)$. However the estimation of the nonlinear function renders impossible in the majority of cases and certain assumptions have to be assumed for quantifying synchronization. Measures such as the mutual information or the phase locking value are examples of nonlinear metrics, the former assuming a certain statistical interdependency between signals and the latter considering only a phase relation. Finally, spectral metrics, such as the coherence or the imaginary part of coherence, translate the problem to the spectral domain, analyzing the relation between the spectra obtained from the original time series assuming linear/nonlinear relations (see [12] for a thorough review about metrics quantifying synchronization in real data sets).

☆ I. Echegoyen would like to thank the Foundation Tatiana Pérez de Guzmán el Bueno for financially supporting this research. R.S.E. acknowledges support from Consejo Nacional de Ciencia y Tecnología call SEP-CONACYT/CB-2016-01, grant number 285909. J.M.B. is supported by Spanish Ministry of Economy and Competitiveness under Projects FIS2013-41057-P and FIS2017-84151-P. J.H.M. acknowledges M. Chavez for his valuable comments.

* Corresponding author at: Universidad Rey Juan Carlos & Center for Biomedical Technology, Calle Tulipan s/n, 28933 Mostoles, Spain.
E-mail address: javier.buldu@urjc.es (J.M. Buldú).

https://doi.org/10.1016/j.chaos.2018.12.006
0960-0779/

In the current paper we are concerned about using ordinal patterns, a symbolic representation of temporal data sets, to define a new metric that is able to reveal the synchronization between time series. This representation is grounded on the transformation of time series into ordinal vectors of a given length D, where the elements of the vector correspond to the order, from the lowest to the highest, of the values of the time series (see Materials and Methods for details). The analysis of the ordinal patterns has been traditionally applied to quantify the amount of stochasticity and determinism in real time series [13,14], allowing to determine the existence of *forbidden patterns*, which consists on specific ordinal patterns that do not appear along the time series under study. This methodology has been applied in a diversity of real systems, since, once the time series are projected into ordinal patterns, the subsequent analysis does not take into account the origins of the patterns. In this way, ordinal patterns of cardiac signals [15], electroencephalographic recordings[16,17], climate networks [18] or lasers [19] have been extracted with the aim of quantifying the entropy and complexity of the time series. However, the analysis of ordinal patterns can also be used to characterize the interplay between dynamical systems. For example, Bahraminasab *et. al.* [20] used a symbolic dynamics approach to design a directionality index parameter. Transforming the increment between successive points within a times series into ordinal patterns, authors calculated the mutual information between a process X_1 at time t and a process X_2 at time $t+\tau$ and next obtained the directionality index as defined in [21]. Applying this methodology to respiratory and cardiac recordings it is possible to quantify how respiratory oscillations have more influence on cardiac dynamics than vice-versa [20]. More recently, Li et al. used a similar indicator to evaluate the directionality of the coupling in time series consisting of spikes [22]. Using the Izhikevich neuron model [23], authors showed how that methodology was robust for weak coupling strengths, in the presence of noise or even with multiple pathways of coupling between neurons. More recently, Rosário *et. al.* [24] used the ordinal patterns observed in EEG datasets, also known as "motifs" [25], to construct time varying networks and analysed their evolution along time and the properties of the averaged functional network. Specifically, the amount of synchronization between a pair of recorded electrodes of an EEG was obtained by evaluating the number of ordinal patterns co-ocurring at the same time but also at a given lag $\lambda = 1$ time steps. Using both positive and negative values of λ authors were able to quantify the direction of the interaction between the two time series, i.e., the causality, to further construct temporal time networks. Next, they showed how the resulting time varying functional networks were able to identify those brain regions related to information processing and found differences between healthy individuals and patients suffering from chronic pain [24].

In this paper, we also propose the use of symbolic dynamics to evaluate the level of synchronization between time series. However, our methodology consists in a measure of synchronization that does not take into account the existence of a delay time between time series, despite further adaptation to this case is also possible (see Section Conclusions). As in the case of [20,24,25], we take advantage of the transformation of a time series into a concatenated series of D-dimensional ordinal patterns [13] that allow us to quantify the amount of synchronization between two (or more) symbols sequences. The main advantage of our methodology is that it takes into account both the in-phase and anti-phase synchronization of two dynamical systems, the latter being disregarded in the aforementioned proposals based on ordinal patterns.

We have calculated the *OS* of two kind of data sets: (i) unidirectionally coupled Lorenz electronic systems and (ii) magnetoencephalographic (MEG) recordings measuring the activity of 241 sensors placed at the scalp of an individual during resting state.

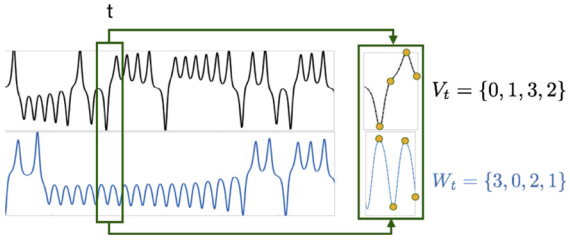

Fig. 1. Qualitative example of ordinal vectors extraction from two time series. Here $D = 4$ is the length of the ordinal patterns. From each time series, an ordinal vector containing the desired number of samples is obtained by ranking its D values at time t, inside the vector.

Next, we compared the amount of synchronization computed by *OS* with respect to those obtained from classical metrics like *phase locking value* (PLV), *mutual information* (MI), *spectral coherence* (SC) and *Pearson correlation* (r). To ensure the results obtained from OS are due to the real underlying synchronization between time series, and not to statistical noise, we have ran a surrogate validation for both datasets. A complete explanation of the procedure can be found in Appendix D.

2. Materials and methods

2.1. Defining ordinal synchronization

To compute the (OS) between two time series X and Y, we first extract their D-dimensional ordinal patterns [13]. In this way, we choose a length D and divide both time series of length M into $L = M/D$ equal segments. Next, we obtain the order of the values included inside each segment, also called the *ordinal patterns*:

$$X_t = \{x_1, x_2, \ldots, x_D\} \mapsto V_t = \{v_1, v_2, \ldots, v_D\} \tag{1}$$

$$Y_t = \{y_1, y_2, \ldots, y_D\} \mapsto W_t = \{w_1, w_2, \ldots, w_D\} \tag{2}$$

where V_t and W_t are the *ordinal vectors* inside the segment given by $\{t, t+1, \ldots, t+D-1\}$, elements refer to the ordinal position of the values in X_t and Y_t, respectively. Note that the elements in V_t and W_t are natural numbers ranging from 0 to $D-1$. The higher the value in the time series, the higher the corresponding element in the ordinal vector. Following the example depicted in Fig. 1, where $D = 4$, we obtain:

$$X_t = \{-1.22, 0.44, 0.91, 0.63\} \mapsto V_t = \{0, 1, 3, 2\} \tag{3}$$

$$Y_t = \{1.34, 0.12, 0.78, 0.57\} \mapsto W_t = \{3, 0, 2, 1\} \tag{4}$$

Then, we take the euclidean norm of each ordinal vector.

$$||V_t|| = \sqrt{v_1^2 + v_2^2 + \ldots + v_D^2} = \sqrt{0^2 + 1^2 + \ldots + (D-1)^2} \tag{5}$$

and we call $V_t^N = V_t/||V_t||$ and $W_t^N = W_t/||W_t||$ the normalized vectors. Note that this step only depends on the length D.

Now, we define the raw value of the *instantaneous ordinal synchronization* at time t (IOS_t^{raw}) as the dot product between both ordinal ordinal vectors $IOS_t^{raw} = \sum_{i=1}^{D} v_{i,t} w_{i,t}$ (i.e., $V_t^N \cdot W_t^N$). For a more intuitive interpretation, we linearly rescale the value of IOS_t^{raw} to be bounded between -1 and 1:

$$IOS_t = 2\left(\frac{IOS_t^{raw} - min}{1 - min} - 0.5\right) \tag{6}$$

where *min* is the minimum possible value of the scalar product between two ordinal vectors. Note that, since the elements of the ordinal vectors are always positive and have only one component equal to zero, the lowest possible scalar product between V_t and

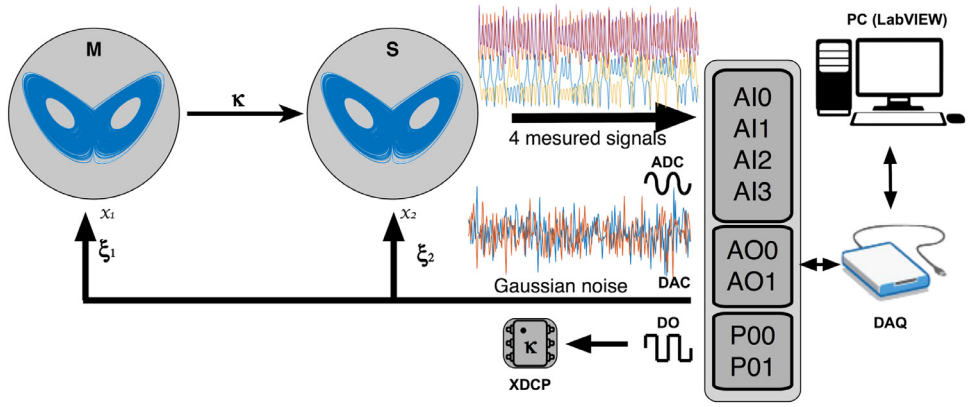

Fig. 2. Schematic representation of Lorenz systems in a master-slave configuration. Signals are measured through a DAQ card (Ports AI0-AI3) and stored in a PC. Digital output (P00-P01) ports and XDCP control the value of coupling strength κ. Analog output ports (AO0-AO1) introduce the external noise signals ξ_1 and ξ_2 perturbing the x_1 master (M) and x_2 slave (S) variables, respectively.

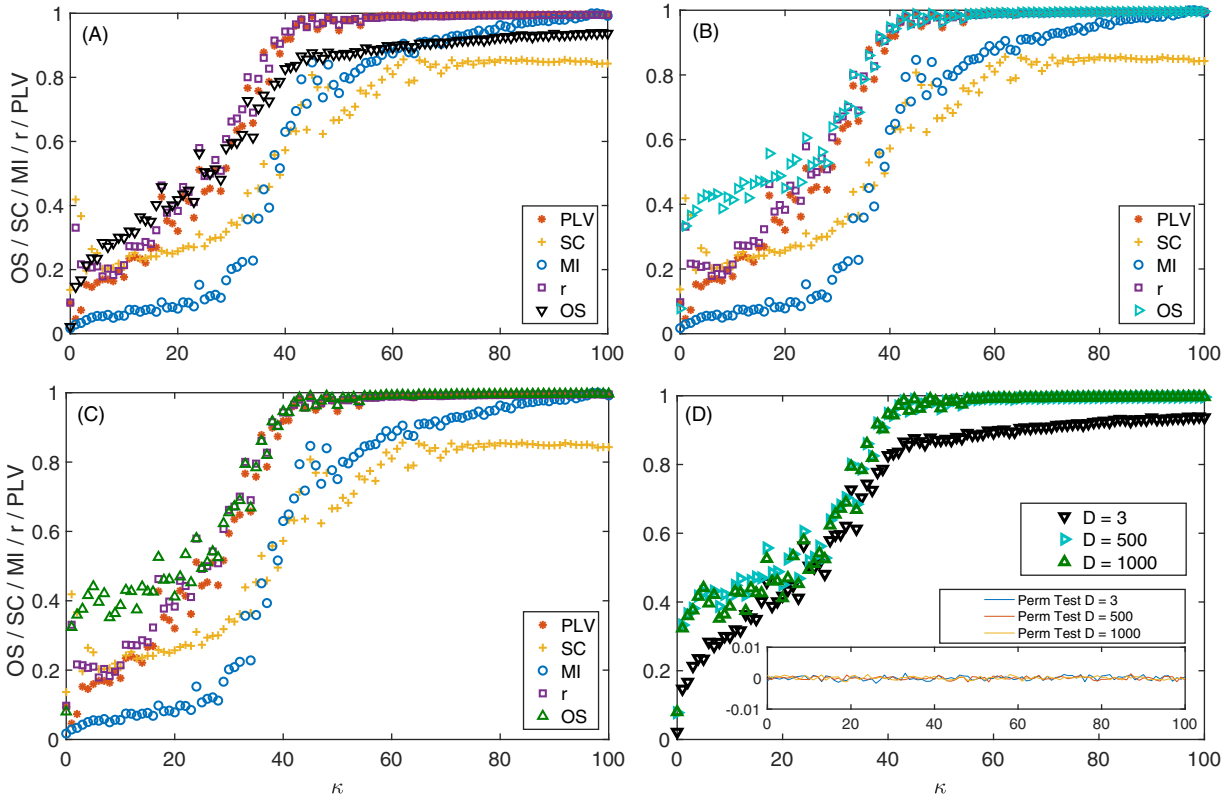

Fig. 3. Synchronization against coupling strength κ as measured with *PLV* (red stars), *SC* (yellow crosses), *MI* (light blue circles), *r* (purple squares). *OS* (triangles) is plotted for $D = 3$ (A) (black downward-pointing), $D = 500$ (B) (turquoise right-pointing) and $D = 1000$ (C) (green upward-pointing). For comparison purposes, plot (D) shows *OS* against κ for different vector lengths, $D = 3$, $D = 500$ and $D = 1000$. The inset shows the results for the permuted time series for $D = 3$, $D = 500$ and $D = 1000$. (For interpretation of the references to colour in this figure legend, the reader is referred to the web version of this article.)

W_t is obtained when the order of the elements of vector V_t is inverted in W_t. In our example:

$$min = \frac{0(4) + 1(3) + 2(2) + 3(1) + 4(0)}{0^2 + 1^2 + 2^2 + 3^2 + 4^2} \tag{7}$$

In general, for any vector of length D:

$$min = \frac{0(D-1) + 1(D-2) + \ldots + (D-2)1 + (D-1)0}{0^2 + 1^2 + \ldots + (D-1)} \tag{8}$$

Following the normalization in 6), we ensure that two ordinal vectors that follow opposite evolutions will unambiguously lead to a value of $IOS_t = -1$, and two vectors whose elements have the same order will have an $IOS_t = 1$. Being $L = M/D$ the total number of ordinal vectors in time series of M points, the final value of the ordinal synchronization $OS\{X, Y\}$ for a given pair of time series X and Y is obtained averaging the instantaneous values of IOS_t along the whole time series:

$$OS\{X, Y\} = \langle IOS_t \rangle \tag{9}$$

Since we consider the IOS_t of consecutive (i.e., non-overlapping) time windows, the value of t in Eq. 9 is given by the expression $t = 1 + iD$, with i being a natural number bounded by $0 \leq i \leq L - 1$. Note that it is also possible to define a *sliding OS* just by increasing t in one unit for every IOS_t instead of considering consecutive windows.

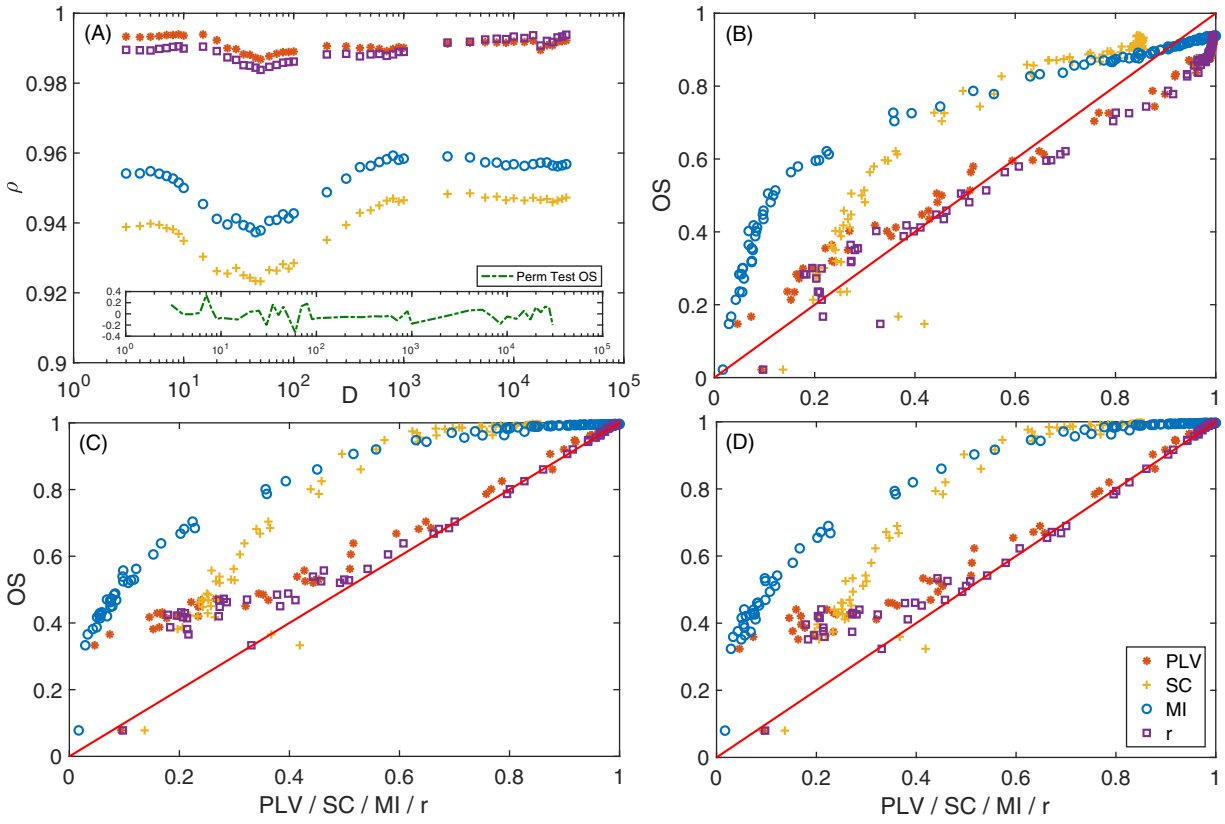

Fig. 4. Panel (A) shows the average correlation (ρ) between each synchronization measure and OS depending on the vector length D. Panels (B)-(D) show the correlation between OS and all other synchronization measures varying the coupling strength (from 0 to 100), for $D = 3$ (B), $D = 500$ (C) and $D = 1000$ (D).Following the same notation as in Fig. 3, synchronization measures are (MI; blue), (r; purple), (SC; yellow) and (PLV; red). The red line corresponds to $y = x$. (For interpretation of the references to colour in this figure legend, the reader is referred to the web version of this article.)

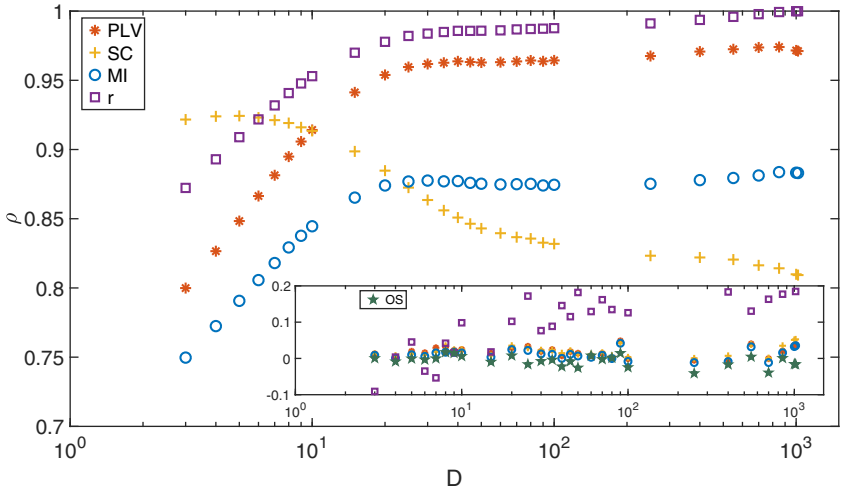

Fig. 5. Correlation ρ between different synchronization metrics and OS as a function of the length D of the ordinal vectors. As in previous figures: PLV (red), SC (yellow), MI (blue), r (purple). The inset depicts the effect on the correlation of permuting the time series. Each point shows the average across 100 iterations. (For interpretation of the references to colour in this figure legend, the reader is referred to the web version of this article.)

2.2. Experimental results: Electronic lorenz systems

We analyzed the transition to the synchronized regime of two coupled Lorenz oscillators [26]. We implemented an electronic version of the Lorenz system, whose equations are detailed in Appendix B. Two Lorenz circuits are coupled unidirectionally in a master-slave configuration (see Fig. 2) with a coupling strength κ that can be modified. Our experiments include two conditions: in the first one, κ is modified in the absence of external noise; in the second one, κ varies in presence of Gaussian noise with band selection. The (AI0-AI3) input ports of a data acquisition (DAQ) card are used for sampling the x and z variables of each circuit, while the output ports AO0 and AO1 generate two different noise signals (ξ_1, ξ_2) that perturb the dynamics of the Lorenz circuits through variable x of each circuit. In this way, an external source of noise can be introduced to check the robustness of the experiments. The circuit responsible of the coupling strength κ is controlled by a digital potentiometer XDCP, which is adjusted by dig-

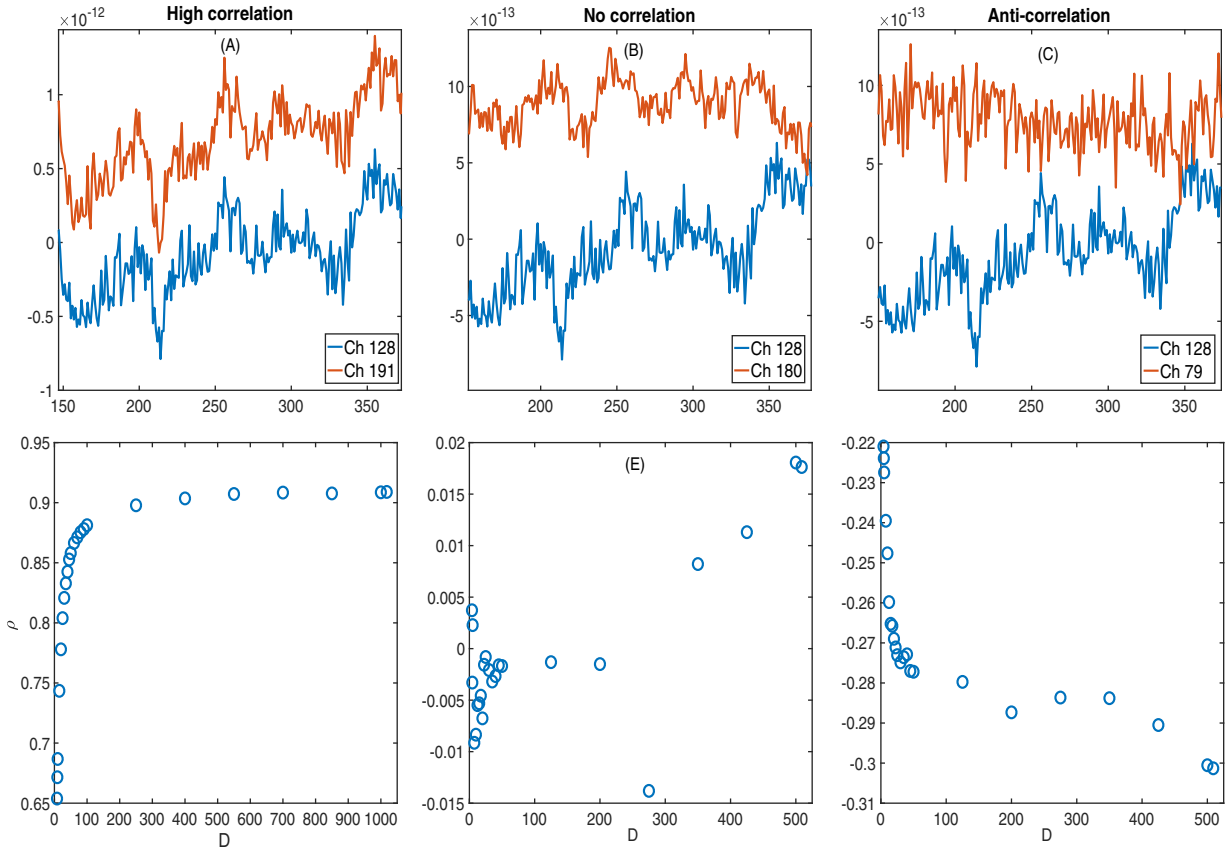

Fig. 6. Example of the MEG time series and their corresponding *OS* vs *D* for three different situations: two sensors with high correlation (A and D), no correlation (B and E) and anti-correlated (C and F). Upper panel shows part of the raw signals recorded at the sensors while bottom panel shows *OS* depending on the length *D*.

ital pulses from ports P00 and P01. Noisy signals were designed in LabVIEW, using a Gaussian White Noise library [27] that generates two different Gaussian-distributed pseudorandom sequences bounded between [-1 1]. All the experimental process is controlled by a virtual interface in LabVIEW 2016 (PC).

The experiment works in the following way: First, κ is set to zero and digital pulses (P00 and P01) are sent to the digital potentiometer until the highest value of κ is reached. Second, variables x and z of the circuits are acquired by the analog ports (AI0-AI3) in order to compute the synchronization metrics. Initially, we have obtained all results for $\xi_1 = \xi_2 = 0$, i.e., in the absence of external noise, and then, after a moderate amount of noise is introduced, all synchronization metrics are calculated again (See Appendix C). Every signal, with or without noise, has a length of 30,000 samples.

2.3. Applications to magnetoencephalographic recordings

We have checked the performance of the *OS* in the context of neuroscientific datasets. Specifically, we quantified the level of synchronization between pairs of channels of MEG recordings. Data sets have been obtained from the Human Connectome Project (for details, see [28] and https://www.humanconnectome.org). The experimental data sets consist of 30 MEG recordings of an individual during resting state for a period of approximately 2 minutes each. During the scan, the subject were supine and maintained fixation on a projected red crosshair on a dark background. Brain activity was scanned with 241 magnetometers on a whole head MAGNES 3600 (4D Neuroimaging, San Diego, CA, USA) system housed in a magnetically shielded room. The root-mean-squared noise of the magnetometers is about 5 fT/sqrt (*Hz*) on average in the white-noise range (above 2 *Hz*). Data was recorded at sampling rate of $f_s \approx 508.63$ *Hz*. Five current coils attached to the subject, in combination with structural-imaging data and head-surface tracings, were used to localize the brain in geometric relation to the magnetometers and to monitor and partially correct for head movement during the MEG acquisition. Artifacts, bad channels, and bad segments were identified and removed from the MEG recordings, which were processed with a pipeline based on independent component analysis to identify and clean environmental and subject's artifacts [28].

3. Results

3.1. Nonlinear electronic circuits

In order to assess the validity of *OS*, we have explored its performance for different values of *D*, from 3 to the full length of the time series under evaluation. Since it is the first time *OS* is used, we have compared it to classical measures of correlation, namely Pearson correlation coefficient (r), spectral coherence (*SC*), phase locking value (*PLV*) and mutual information (*MI*). We have used two kinds of data sets to validate *OS*, on the one hand, experimental time series from nonlinear electronic circuits, and on the other hand, MEG recordings.

First, we take advantage of the ability of controlling the coupling strength between electronic circuits and investigate how *OS* changes as two dynamical systems smoothly vary their level of synchronization from being unsynchronized to completely synchronized. Specifically, two electronic Lorenz systems are unidirectionally coupled with a parameter κ controlling their coupling strength (see Appendix B for details). Initially, we do not perturb

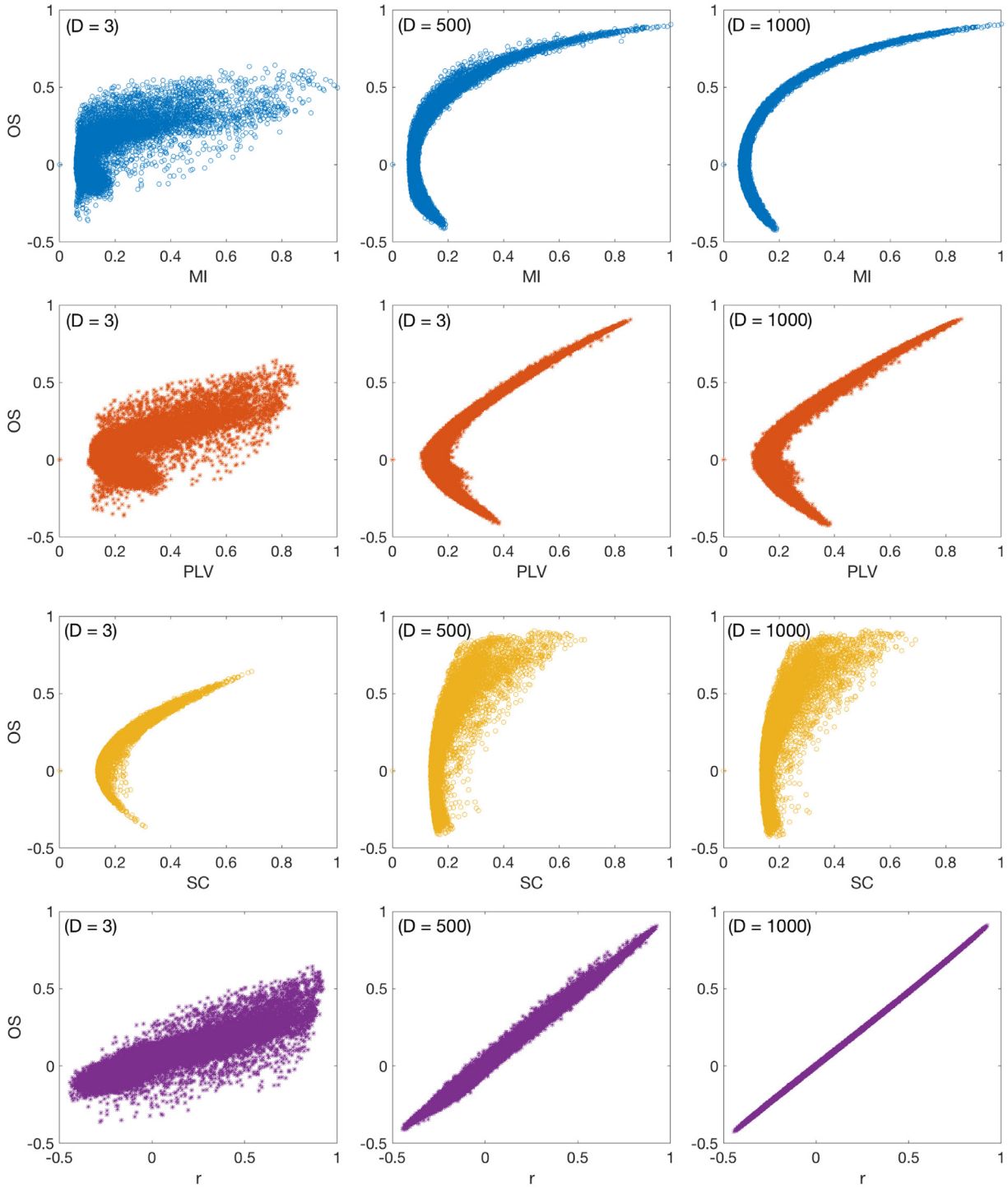

Fig. 7. Correlation between *OS* and other synchronization metrics in MEG data sets. The color code is preserved: *MI* (upper row, blue), *PLV* (second row, red), *SC* (third row, yellow) and *r* (bottom row, purple). Each column corresponds to an *OS* obtained with different lengths D of the ordinal vectors: $D = 3$ (left column), $D = 500$ (middle column) and $D = 1000$ (right column). (For interpretation of the references to colour in this figure legend, the reader is referred to the web version of this article.)

the oscillators with external noise (see Appendix C for the case of including external noisy signals). However, we cannot avoid the intrinsic noise of the electronic circuits together with the tolerance of the electronic components (between 5% and 10%). Fig. 3 shows how the value of *OS* changes as the coupling strength κ is increased from zero. Since the value of *OS* depends on the length of the ordinal vectors, we show the results for three different values: $D = 3$ (Fig. 3A), $D = 500$ (Fig. 3B) and $D = 1000$ (Fig. 3C). Note that, by increasing the length of the vectors, we are obtaining the amount of synchronization at different time scales. Together with *OS*, we plot the values of the rest of synchronization metrics in (A), (B) and (C), which remain unaltered in the three plots (since they do not depend on D). To get an overall view of the effect of D on the resulting value of OS and its ability to capture the underlying synchronization, we ran a surrogate test with one hundred iterations for all values of κ (see Appendix D), and plot the results of the test (inset) along with $D = 3$, $D = 500$ and $D = 1000$ (Fig. 3D).

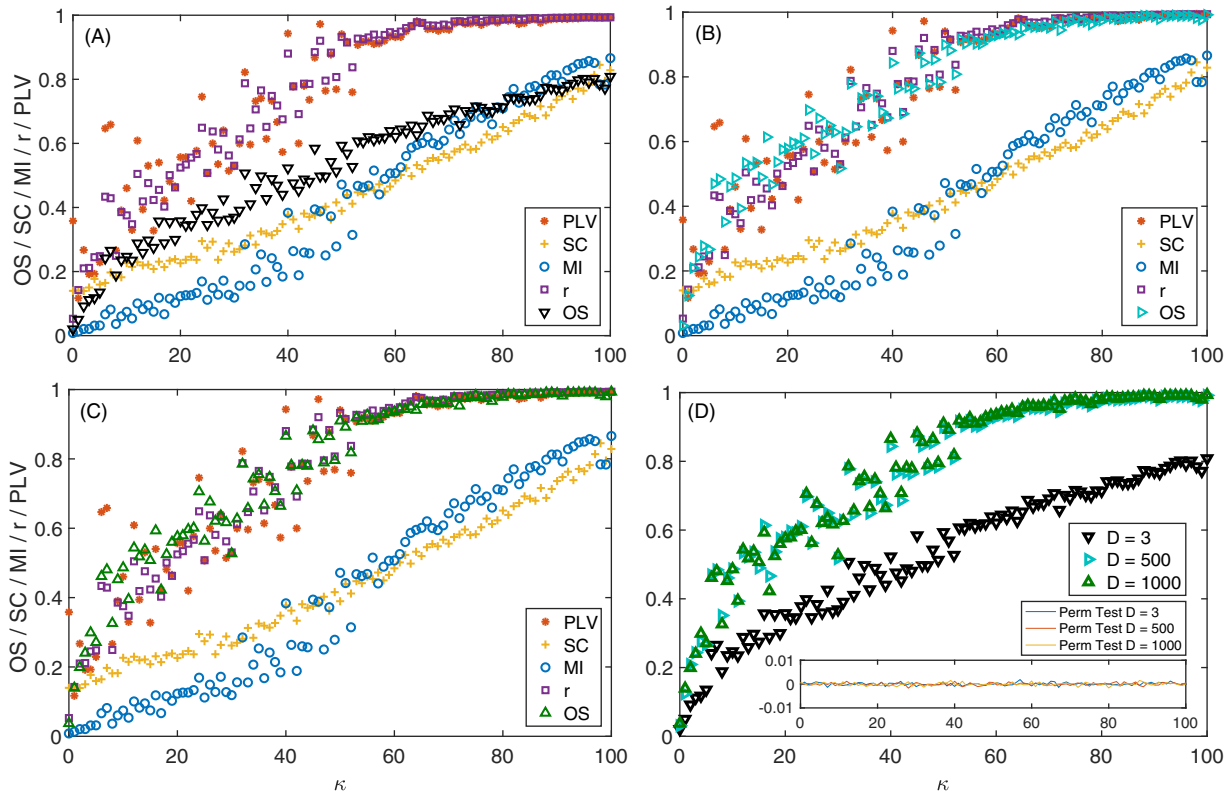

Fig. 8. Synchronization against coupling strength κ, as measured with mutual information *MI* (light blue), spectral coherence *SC* (yellow), phase locking value *PLV* (red) Pearson correlation *r* (purple) and ordinal synchronization *OS* (black) for $D = 3$ (A), $D = 500$ (B) and $D = 1000$ (C). For comparison purposes, plot *D* shows *OS* against coupling strength for the different vector lengths, $D = 3$ (black), $D = 500$ (turquoise) and $D = 1000$ (green). (For interpretation of the references to colour in this figure legend, the reader is referred to the web version of this article.)

In all cases, we observe that *OS* increases for low to moderate values of κ and remains at a high value once a certain threshold is reached. This behaviour is similar to the rest of the synchronization metrics. However, both *MI* and *SC* seem to saturate at values of κ higher than *r, PLV* and *OS*, which seem to reach a plateau around $\kappa = 40$. Fig. 3D shows the comparison of *OS* for the three different values of *D* and the surrogate test (inset). Here, we can also observe how at $D = 3$, *OS* has a different qualitative behaviour from $D = 500$ and $D = 1000$, since it stays around 0.9 and does not reach 1 as in the windows of longer lengths. The reason is the existence of intrinsic noise of the electronic circuits, that affects much more the alignment of the ordinal vectors of shorter lengths than those with higher dimensions. When we permute the time series and recalculate synchronization, *OS* tends to zero, no matter the value of κ or *D* (inset of Fig. 3D). This is equivalent to test the values *OS* in the case of no temporal coordination, given the actual distribution of values in the time series. As shown in the figure, in such a situation, *OS* is indicating that there is no synchronization (values around 0), confirming *OS* is driven by the underlying coordinated dynamics and not by statistical noise.

Fig. 4 shows the average correlation (ρ) between each D-dependent *OS* and the rest of synchronization metrics with zero noise. Note that correlations are higher than 0.92 in all cases, although it seems to be certain vector lengths that maximize these correlations. Also note that correlations with *PLV* and *r* are the highest and, in all cases, very close to 1. At the same time, *MI* and *SC* show lower correlations that, in turn, seem to be more dependent on the value of the vector length *D*. On the contrary, the correlation when time series are permuted decays below ± 0.4 (see Fig. 4A).

We can investigate how *OS* is related to the rest of the synchronization metrics in more detail by setting the length of the ordinal vectors to a given value (3, 500 or 1000 in this case) and observe the influence of the level of synchronization (Fig. 4B, C and D). For any of the three selected lengths, *OS* shows a linear relation with *PLV* and *r*, especially at values of *OS* higher than 0.5. However, the relation with *SC* and *MI* seems to be nonlinear in all cases. Interestingly, for low levels of synchronization, *OS* increases much faster than these two latter metrics. While *SC* saturates around 0.8, *MI* finally increases faster than *OS* only for high values of synchronization, eventually reaching the value of *OS* around 1. Also note how, in the case of $D = 3$ (Fig. 4B), the intrinsic noise of the electronic circuits prevents *OS* to reach the value of one. This behaviour can be observed even clearer in the case of adding more noise into the system, as shown in Appendix C.

3.2. MEG Signals

The second application is the evaluation of the level of synchronization between the 241 sensors measuring the activity of an individual during resting state. Concretely, we have 30 recordings of 2 minutes each. In this case, we cannot control the amount of coupling between sensors but, alternatively, we have a diversity of levels of synchronizations between all possible pairs of sensors. Fig. 5 shows how the correlations between *OS* and the rest of the metrics change depending on *D*. As we can observe, correlations are high in all cases except for *SC*, but this one saturates around the same *D* as the other synchronizations does. The inset of the figure shows the correlations with the values of OS after permuting the time series. Each point shows the average of 100 realizations.

As in the case of the electronic Lorenz oscillators, tuning the value of *D* allows to obtain values of *OS* closer, or more correlated, to other metrics. In fact, two different regions are clearly observed: (i) for values of $D \leq 20$ the correlation of *OS* with PLV, r, and MI in-

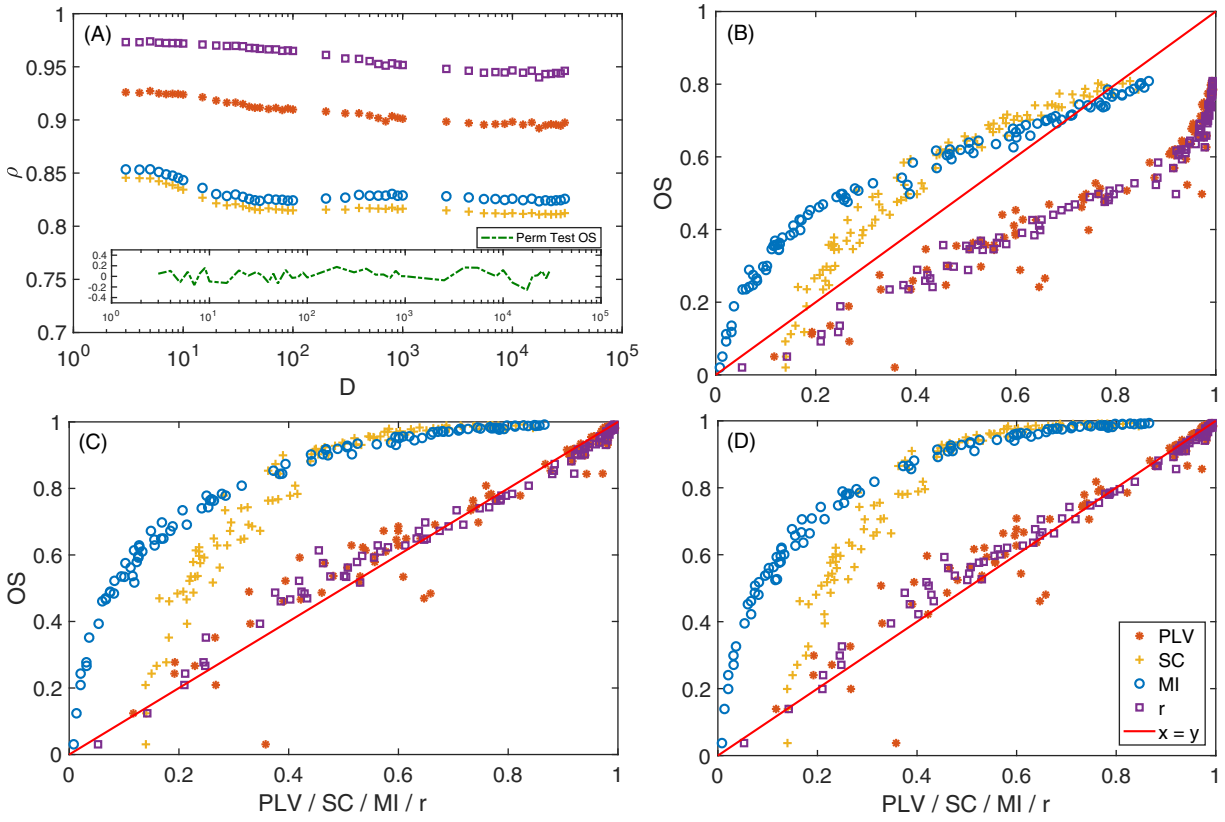

Fig. 9. Panel A shows the average correlation between each synchronization measure and OS depending on the vector length (D) used to compute OS. Panels B-D show the correlation between OS and all other synchronization measures varying the coupling strength (from 0 to 100), for $D = 3$ (B), $D = 500$ (C) and $D = 1000$ (D). Synchronization measures are Mutual information (MI; blue), Pearson correlation coefficient (r; purple), spectral coherence (SC; yellow) and phase locking value (PLV; red). The red line corresponds to $y = x$. (For interpretation of the references to colour in this figure legend, the reader is referred to the web version of this article.)

creases with D, while (ii) for $D > 20$ correlation saturates around the highest value, being r the metric with the highest correlation. Interestingly, the behaviour of the SC goes in the opposite direction, decreasing for higher values of D. Again, this correlation disappears when time series are shuffled, indicating that OS is related to the real synchronous state of the system and to random fluctuations.

In order to gain insights about how the behaviour of *OS* depends on the level of synchronization and the length D, we plot three different cases in Fig. 6. In (A), we show the time series of two highly-correlated sensors, with their corresponding *OS* value depending on D (Fig. 6D). Plot (B) and (C) show the cases of two uncorrelated and negatively correlated sensors, respectively, with their values of *OS* (Figs. 6E and F). Note that for the positive (negative) case, correlations tend to stabilize as D grows, indicating the existence of a certain temporal scale at which synchronization is increased (reduced). Also note that, when time series are not correlated, this pattern is not that clear, and *OS* values remain low for any value of D.

We had analyzed the relation of *OS* with the rest of the metrics according to the level of synchronization. Fig. 7 shows a panel of plots capturing the correlations between *OS* and all other synchronization metrics for the MEG signals. Left plots show the case of $D = 3$, middle plots show $D = 500$ and right plots show $D = 1000$. Different conclusions can be drawn depending on the synchronization metric *OS* is compared to. In the case of *MI* (first row), the existence of a nonlinear correlation between both metrics arises. However, this correlation decreases with the length of the ordinal vectors, becoming rather noisy for $D = 3$. This behaviour is induced by the intrinsic noise of the MEG signals that, as in the case of electronic circuits, affects the value of *OS* when short lengths of the ordinal vectors are considered. Also note that *MI* is not able to distinguish positive from negative correlations between time series, a fact that makes *OS* an interesting metric when both kind of synchronizations are expected. In our case, for example, despite the highest values of *OS* are close to 1, the lowest ones arrive to -0.35, indicating the existence of anti-correlated dynamics between certain pairs of sensors. A similar behaviour is reported in the case of the comparison with *PLV* (second row). Again, a nonlinear relation exists between both metrics, which is rather noisy at low values of the ordinal vector lengths ($D = 3$). *PLV* has also the same limitations as *MI*, since it does not differentiate between positive and negative correlations. Interestingly, the relation with *SC* is different from the two previous metrics (third row). Despite a nonlinear correlation between *OS* and *SC* seems to be present in the plots, this correlation is deteriorated with the increase of D.

Finally, *OS* shows a clear linear correlation with r (bottom row), which, as in the case of *MI* and *PLV* becomes noisy for low values of D. Note that, the loss of correlation for low values of D is indicating that, at short time scales, *OS* is capturing a different pattern of synchronization than at large scales. This is an interesting feature of *OS* which suggests that, when using it as a metric to evaluate synchronization between signals, it is appealing to carry out an analysis depending on the vector length in order to reveal the existence of different levels of synchronization at different time scales.

4. Conclusions

We have introduced the *Ordinal Synchronization* (*OS*), a new metric to evaluate the level of synchronization between time series by means of a projection into ordinal patterns. We have checked the performance of OS with two kinds of experimental data sets obtained from: (i) unidirectionally coupled nonlinear electronic circuits and (ii) 30 magnetoencephalographic recordings containing the signals of 241 channels. Additionally, we performed a surrogate test to unveil the extent to which *OS* is affected by random fluctuations, preserving the distribution of values in the time series, but shuffling its order. In all cases, values of *OS* tend to zero, and correlations with other measures decay below 0.2. We conclude that *OS* is driven by inner synchronous states of the system, with only mild impact of the random fluctuations given in the time series.

There are several advantages of using *OS*. First, it is able to capture in-phase and anti-phase synchronization. Second, tuning the length of the ordinal vectors D, it is possible to evaluate the level of synchronization at different time scales. Third, it is not necessary to assume any *a priori* property of the time series, such as stationarity or linear coupling. Fourth, the calculation of *OS* is extremely fast, especially when compared with other metrics such as *MI*. On the other hand, we have also seen that one of the elements affecting the value of *OS* is the existence of noise, which reduces its value if the dimension of the ordinal vectors is low. However, depending on the application, this fact can also be considered as an indicator of the existence of noise.

A comparison with other classical metrics to evaluate synchronization has been carried out showing some similarities and differences. In general, *OS* shows high correlation with *r* and *PLV*, something that can be explained by the way *OS* is constructed. Ordinal patterns filter part of the information contained in the amplitude of the signal, maintaining just the ranking in the time series. This is something between considering just the phase (*PLV*) or just the amplitude (*r*), since differences in amplitude are not related to changes in the *OS* parameter as long as the ranking is not modified.

It is worth noting that OS still has some properties that need to be investigated in detail. On the one hand, it is not clear what is the interplay between the length D of the ordinal vectors and the characteristic frequencies of the time series. Several studies have shown how the auto-correlation of the time series is related to the percentage of appearance of certain ordinal patterns [17,29,30]. However, these references only consider a length $D = 3$, which allows to perceive a change in the frequency of appearance of the patterns but does not reveal what the consequences are for higher D. In that sense, our methodology (i.e., the quantification of OS at different values of D) could provide a full analysis of the synchronization at different time scales. On the other hand, note that the number of ordinal vectors decreases with D, which worsens the statistics for high values of D. Specifically, for $D = 1000$, we obtain 30 ordinal vectors for both the case of the Lorenz electronic circuits and the MEG recordings. However, despite the number of vectors is much lower than the case of, e.g. $D = 3$, we have enough realizations to evaluate the synchronization between ordinal vectors. Importantly, since we are not evaluating the number of ordinal patterns appearing in the time series, 30 ordinal vectors is a reasonable number to evaluate whether two time series are synchronized, or not, since it would be equivalent to, for example, repeating 30 times a given experiment. Finally, further studies extending the concept of OS could address the quantification of n: m synchronization. For example, the methodology we propose could be adapted to evaluate the alignment of vectors embedded with a time delay τ [31], which could uncover synchronization at n: m ratios.

In view of all, we believe that the use of *OS* can be interesting (but not restricted to) for evaluating the amount of synchronization in neuroscientific data sets, where in-phase and anti-phase synchronization are know to co-exist, together with coordinations at different time scales.

Appendix A. Coordination metrics

A.1. Pearson's Correlation Coefficient

The Pearson's correlation coefficient r consists of a covariance scaled by variances, thus capturing linear relationships among variables. From the equations of the variance (of X and Y) and covariance (of XY), we obtain Pearson Correlation Coefficient as:

$$S_Y = \sqrt{\frac{\sum (Y_i - \bar{Y})^2}{n-1}} = \sqrt{\frac{\sum y_i^2}{n-1}} \tag{10}$$

$$S_X = \sqrt{\frac{\sum (X_i - \bar{X})^2}{n-1}} = \sqrt{\frac{\sum x_i^2}{n-1}} \tag{11}$$

$$S_{XY} = E[(X - E[X])(Y - E[Y])] \tag{12}$$

$$r = \frac{S_{XY}}{S_X S_Y} \tag{13}$$

Pearson's correlation is a measure of linear dependence between any pair of variables and it has the advantage of not requiring the knowledge of how variables are distributed. However, it should be applied only when variables are linearly related to each other.

A.2. Coherence

Coherence (magnitude squared coherence or coherence spectrum) measures the linear correlation among the two spectra[12]. To calculate the coherence spectrum, data must be in the frequency domain. In order to do so, time series are usually divided into S sections of equal size. The Fast Fourier Transform algorithm is then computed over the sections to get the estimate of each section's spectrum (periodogram). Then, the spectra of the sections is averaged to get the estimation of the whole data's spectrum (Welch's method). Finally, Coherence is a normalization of this estimate by the individual autospectral density functions [12]:

$$SC = \frac{|\langle Sp_{xy}^2 \rangle|}{|\langle Sp_{xx} \rangle||\langle Sp_{yy} \rangle|} \tag{14}$$

where Sp_{xy} is the Cross Power Spectral Density (CPSD) of both signals, Sp_{xx} and Sp_{yy} are the Power Spectral Density (PSD) of the segmented signals X and Y taken individually, and $\langle \cdot \rangle$ is the average over the S segments. In the case of the data sets obtained with the nonlinear electronic Lorenz systems, frequencies higher than $f_{cut} = 7.5K$ Hz have been disregarded for the computation of *SC*, since the power spectra of the electronic circuits are completely flat above this frequency. One of the drawbacks of Coherence is that it doesn't discern the effects of amplitude and phase in the relationships measured between two signals, which makes its interpretation unclear [4,32].

A.3. Phase Locking Value

Phase Locking Value was first introduced by Lachaux et al. [32] as a new method to measure synchrony among neural populations. It has, at least, two major advantages over the classical coherence measure: it doesn't require data to be stationary, a condition that can rarely be validated; and has a relatively easy interpretation (in terms of phase coupling). However, the methods used to extract instantaneous phase, a step needed to calculate *PLV* rely on stationarity, so indirectly *PLV* can be affected by this condition

[33]. To obtain the *PLV*, the signal has to be decomposed to it's instantaneous phases and amplitudes. To achieve this, there are several methods, such as Morlet wavelet convolution or Hilbert transform [12,33]. In this work we will utilize the latter. Finally, *PLV* is obtained averaging over time t:

$$PLV = \frac{1}{N}\left|\sum_{n=1}^{N}\exp\left(i\theta(t,n)\right)\right| \tag{15}$$

where $\theta(t, n)$ is the (instantaneous) phase difference $\phi_x - \phi_y$, the phases to be compared from the signals X and Y. Comparisons are carried out pairwise (bivariate).

A.4. Mutual Information

Mutual Information is a measure of shared information between any components of a system, between systems, or any other parameter whose value's probability can be estimated. It is based on Shannon's notion of entropy, which, in a general sense, tries to quantify the amount of information contained in a random variable by means of its estimated probability distribution. Mutual information measures the amount of information *shared* between two random variables by means of its joint distribution, or conversely, the amount of information we can obtain from one random variable observing another. This is analogue to measuring the dependence between two random variables [34]. Let X and Y be two random variables with $\{x_1, x_2, \ldots x_n\}$ and $\{y_1, y_2, \ldots y_n\}$, n possible values with probabilities $p(x)$ and $p(y)$. The *MI* of X relative to Y can be written as:

$$MI(X \cap Y) = \sum_{x\in X, y\in Y} p(x\cap y)\log_2\frac{p(x\cap y)}{p(x)p(y)} \tag{16}$$

$$MI(X \cap Y) = H(X) - H(X|Y) \tag{17}$$

where $p(x\cap y)$ is the probability that X has a value of x *while* Y has a value of y, $H(X)$ is the entropy of X and $H(X|Y)$ is the conditional entropy of X and Y. One of the major advantages of *MI* is that it captures linear and non-linear relationships among variables. One disadvantage is that it does not explicitly tell the shape of that distribution [33]. To get the mutual information between two random variables, we first need to estimate their probability density distribution [33–35]. Eq. (16) compares joint probabilities against marginal ones. When two values are independent, the product of their marginal probabilities should equal their joint probability. When not, we can state that there is a relationship among them (not necessarily linear), because the probability of finding those values together is greater than the probability of finding them by chance. Thus, somehow, those time series are coupled, although we don't know the way it occurs.

Appendix B. Electronic version of the Lorenz system

The equations of the master and slave electronic Lorenz systems are:

$$V\dot{x}_1 = \frac{1}{R_1C}\left(\frac{R_1}{R_2}V_{y_1} - \frac{R_4}{R_3}V_{x_1} + \frac{R_4}{R_3}V_{\xi_1}\right) \tag{18}$$

$$V\dot{y}_1 = \frac{1}{R_5C}\left(\frac{R_5}{R_6}V_{x_1} - \frac{R_5}{R_7}V_{x_1}V_{z_1}\right) \tag{19}$$

$$V\dot{z}_1 = \frac{1}{R_8C}\left(\frac{R_8}{R_9}V_{x_1}V_{y_1} - \frac{R_{11}}{R_{10}}V_{z_1}\right) \tag{20}$$

$$V\dot{x}_2 = \frac{1}{R_{12}C}\left(\frac{R_{12}}{R_{13}}V_{y_2} - \frac{R_{15}}{R_{14}}V_{x_2} + \frac{R_{12}}{R_{29}}V_{\xi_2} + \frac{R_{12}}{R_{30}}V_{sinx}\right) \tag{21}$$

$$V\dot{y}_2 = \frac{1}{R_{16}C}\left(\frac{R_{17}}{R_{16}}V_{x_2} - \frac{R_{17}}{R_{20}}V_{x_2}V_{z_2}\right) \tag{22}$$

Table 1
Parameters of the electronic components used for the construction of the Lorenz oscillators and the coupled circuit.

$R_1, R_{12} = 100K\Omega$	$R_2, R_{13} = 100K\Omega$	$R_3, R_{14} = 10K\Omega$
$R_4, R_{15} = 10K\Omega$	$R_5, R_{16} = 1M\Omega$	$R_6, R_{17} = 35.7K\Omega$
$R_7, R_{18} = 20K\Omega$	$R_8, R_{19} = 375K\Omega$	$R_9, R_{20} = 20K\Omega$
$R_{10}, R_{21} = 10K\Omega$	$R_{11}, R_{22} = 10K\Omega$	$R_{23} = 10K\Omega$
$R_{24} = 10K\Omega$	$R_{25} = 10K\Omega$	$R_{26} = 10K\Omega$
$R_{27} = 10K\Omega[0–1]$	$R_{28} = 100K\Omega$	$R_{29} = 100K\Omega$
$R_{30} = 100K\Omega$	$C_{1-6} = 1nF$	$V+ = 15V, V- = -15V$

$$V\dot{z}_2 = \frac{1}{R_{19}C}\left(\frac{R_{19}}{R_{20}}V_{x_2}V_{y_2} - \frac{R_{22}}{R_{21}}V_{z_2}\right) \tag{23}$$

where $V_{x_{1,2}}$, $V_{y_{1,2}}$ and $V_{z_{1,2}}$ are the voltage variables of the master (sub-index 1) and slave (sub-index 2) Lorenz systems, $V_{in} = V_{x_1} - V_{x_2}$ is the coupling signal injected into the slave system in a diffusive way, $\kappa = \frac{R_{dp}}{C_5R_{30}}$ is the coupling strength and $0 \le R_{dp} \le 1$ is the percentage of coupling controlled by the digital potentiometer. In the experiments where external noise is considered (see Appendix C), the amplitude of V_{ξ_1} and V_{ξ_2} are set to 0.5 V and zero otherwise.

Table 1 contains the parameters of the resistances and capacitances used in the experiments.

Appendix C. Robustness of *OS* in the presence of external noise

Figs. 8–9 are equivalent to Figs. 3–4 but in the presence of external noise. In this case, we have introduced two noises ξ_1 and ξ_2 perturbing the x_1 and x_2 variables of the master and slave Lorenz systems as explained in Appendix B. Comparing Figs. 3 and 8 we can observe that all synchronization metrics have reduced their values in the presence of external noise, however, the behaviour remains qualitatively similar to the one reported in Fig. 3. Again, the case $D = 3$ is the one suffering the most from the presence of noisy signals (Fig. 8D). When comparing *OS* with the rest of synchronization metrics (Fig. 9), we can also observe a reduction of the correlations respect to the case without external noise. Again, r and *PLV* are the metrics showing higher correlation with *OS*, having a linear correlation for $D = 500$ and $D = 1000$. This correlation is impaired for $D = 3$, since it corresponds to the ordinal vector length that is more affected by noise. On the other hand, the nonlinear correlations with *MI* and *SC* remain quite similar as in the case of the absence of external noise.

Appendix D. Surrogate validation

To double-check whether OS is sensitive to the temporal structure of the dynamical coordination between time series, and to what extent it is affected by statistical noise, we have ran an additional surrogate test for both datasets (Lorenz and MEG recordings). The procedure to generate the surrogated time series is the simplest case of *constrained realisations* without replacement [36]. For this concrete purpose, in which we are not testing the nonlinearity nor the nonstationarity of each time series individually, it is sufficient to simply randomize one of each pair to be compared, thus building a null model of no temporal coordination between them.

The procedure goes as follows: we set a seed and run the MATLAB built-in algorithm "twister" to get a random rearrangement of the indexes for one time series. We then compute the synchronization between one time series in its original order and the shuffled one. We do this process one hundred times for each explored D and every pair of time series. In this way, we ensure that we are breaking temporal relations between time series (coordination), while preserving the distribution of values in each individual

time series. After repeating the process one hundred times, we get the empirical distribution of values of OS we could expect if there were no temporal structure in the dynamics.

Given that we just want to check OS's sensitivity to statistical noise to validate the measure, we will confine ourselves to a descriptive analysis of surrogate testing, ensuring it reacts as expected. However, the results obtained from surrogate testing could be used to establish an offset for empirical results (as a normalizing value), or as a null model to test the statistical significance of each value of OS. As the number of permutation iterations increases, the values obtained approach a normal distribution, that can be used as a null model distribution under the hypothesis of no temporal coordination between time series. Getting the empirical probabilities from that distribution allows one to test whether or not any empirical value of OS, extracted from the same two time series without shuffling are statistically significant. If anyone were to use our measure to analyse synchronization in time series, we strongly recommend to run this same surrogate test to ensure reliability and robustness of the results.

Supplementary material

Supplementary material associated with this article can be found, in the online version, at doi:10.1016/j.chaos.2018.12.006.

References

[1] Huygens C. In oeuvres completes de christian huygens. edited by M Nijhoff (Societe Hollandaise des Sciences, The Hague, The Netherlands) 1893;5:246.
[2] Néda Z, Ravasz E, Brechet Y, Vicsek T, Barabási A-L. Self-organizing processes: the sound of many hands clapping. Nature 2000;403:849–50.
[3] Schmidt R, Carello C, Turvey MT. Phase transitions and critical fluctuations in the visual coordination of rhythmic movements between people. J Exp Psychol Hum Percept Perform 1990;16(2):227–47.
[4] Varela F, Lachaux J, Rodriguez E, Martinerie J. The brainweb: phase synchronization and large-scale integration. Nat Rev Neurosci 2001;2:229–39.
[5] Agladze N, Halaidych O, Tsvelaya V, Bruegmann T, Kilgus C, Sasse P, et al. Synchronization of excitable cardiac cultures of different origin. Biomater Sci 2017;5:1777.
[6] Romer K. Time synchronization in ad hoc networks. in: Proceedings of ACM symposium on mobile Ad Hoc networking and computing (MobiHoc) 2001:173–82.
[7] Wang B, Suzuki H, Aihara K. Enhancing synchronization stability in a multi-area power grid. Sci Rep 2016;6:26596.
[8] Arenas A, Díaz-Guilera A, Kurths J, Moreno Y, Zhou C. Synchronization in complex networks. Phys Rep 2008;469(3):93–153. doi:10.1016/j.physrep.2008.09.002.
[9] Boccaletti S, Latora V, Moreno Y, Chavez M, Hwang DU. Complex networks: structure and dynamics. Phys Rep 2006;424(4–5):175–308. doi:10.1016/j.physrep.2005.10.009.
[10] Mones E, Araújo N, Vicsek T, Herrmann H. Shock waves on complex networks. Sci Rep 2014;4:4949.
[11] Rech C, Perret R. Adding dynamics to the human connectome project with MEG. Int J Syst Sci 1990;21:1881.
[12] Pereda E, Quiroga RQ, Bhattacharya J. Nonlinear multivariate analysis of neurophysiological signals. Prog Neurobiol 2005;77(1–2):1–37. doi:10.1016/j.pneurobio.2005.10.003.
[13] Bandt C, Pompe B. Permutation entropy: a natural complexity measure for time series. Phys Rev Lett 2002;88(17):174102. doi:10.1103/PhysRevLett.88.174102.
[14] Amigó J, Zambrano S, Sanjuán M. Combinatorial detection of determinism in noisy time series. Europhys Lett 2008;83:60005.
[15] Parlitz U, Berg S, Luther S, Schirdewan A, Kurths J, Wessel N. Classifying cardiac biosignals using ordinal pattern statistics and symbolic dynamics. Comput Biol Med 2012;42:319–27.
[16] Keller K, Unakafov AM, Unakafova VA. Ordinal patterns, entropy, and EEG. Entropy 2014;16:6212–39.
[17] Bandt C. A new kind of permutation entropy used to classify sleep stages from invisible EEG microstructure. Entropy 2017;19:197.
[18] Barreiro M, Marti A, Masoller C. Inferring long memory processes in the climate network via ordinal pattern analysis. Chaos 2011;21:013101.
[19] Tiana-Alsina J, Buldú JM, Torrent MC, García-Ojalvo J. Quantifying stochasticity in the dynamics of delay-coupled semiconductor lasers via forbidden patterns. Phil Trans R Soc A 2010;368:367–77.
[20] Bahraminasab A, Ghasemi F, Stefanovska A, McClintock P, Kantz H. Direction of coupling from phases of interacting oscillators: a permutation information approach. Phys Rev Lett 2008;100:084101.
[21] Paluš M, Stefanovska A. Direction of coupling from phases of interacting oscillators: an information-theoretic approach. Phys Rev E 2003;67:055201.
[22] Li Z, Ouyang G, Li D, Li X. Characterization of the causality between spike trains with permutation conditional mutual information. Phys Rev E 2011;84:021929.
[23] Izhikevich E. Simple model of spiking neurons. IEEE Trans Neural Netw 2003;14:1569.
[24] Rosário R, Cardoso P, Muñoz M, Montoya P, Miranda J. Motif-synchronization: a new method for analysis of dynamic brain networks with eeg. Phys A 2015;439:7–19.
[25] Olofsen E, Sleigh J, Dahan A. Permutation entropy of the electroencephalogram: a measure of anaesthetic drug effect. Br J Anaesth 2008;101:810–821.
[26] Lorenz E. Deterministic nonperiodic flow. J Atmos Sci 1963;20:130–41.
[27] National instruments. Noise 2018. http://zone.ni.com/reference/
[28] Larson-Prior L, Oostenveld R, Della Penna S, Michalareas G, Prior F, Babajani-Feremi A, et al. Adding dynamics to the human connectome project with MEG. Neuroimage 2013;80:190–201.
[29] Reinoso JA, Torrent MC, Masoller C. Analysis of noise-induced temporal correlations in neuronal spike sequences. Eur Phys J Specl Topics 2016;225:2689–96.
[30] Masoliver M, Masoller C. Sub-threshold signal encoding in coupled fitzhugh–Nagumo neurons. Sci Rep 2016;8:8276.
[31] Zunino L, Soriano MC, Fischer I, Rosso OA, Mirasso CR. Permutation-information-theory approach to unveil delay dynamics from time-series analysis. Phys Rev E 2010;82:046212.
[32] Lachaux JP, Rodriguez E, Martinerie J, Varela FJ. Measuring phase synchrony in brain signals. Hum Brain Mapp 1999;8(4):194–208. doi:10.1002/(SICI)1097-0193(1999)8:4<194::AID-HBM4)3.0.CO;2-C.
[33] Cohen MX. Analyzing neural time series data: theory and practice. Cambridge, Massachusetts: MIT Press; 2014.
[34] Veyrat-Charvillon N, Standaert F-X. Mutual information analysis: how, when and why? Cryptographic Hardware and Embedded Systems-CHES 2009 Lecture Notes in Computer Science (LNCS) 2009;5747:429–43.
[35] Gierlichs B, Batina L, Tuyls P, Preneel B. Mutual information analysis a generic side-Channel distinguisher. Cryptographic Hardware and Embedded Systems-CHES 2008 Lecture Notes in Computer Science 2008;5154:426–42.
[36] Schreiber T, Schmitz A. Surrogate time series 1999 http://xxx.lanl.gov/pdf/chao-dyn/9909037v1.